Characterization of a novel voltage-dependent outwardly rectifying anion current in Caenorhabditis elegans oocytes

Xiaoyan Yin, Jerod Denton, Xiaohui Yan and Kevin Strange

Am J Physiol Cell Physiol 292:269-277, 2007. First published Aug 9, 2006;
doi:10.1152/ajpcell.00298.2006

Am J Physiol Cell Physiol 292: C269–C277, 2007.
First published August 9, 2006; doi:10.1152/ajpcell.00298.2006.

Characterization of a novel voltage-dependent outwardly rectifying anion current in *Caenorhabditis elegans* oocytes

Xiaoyan Yin, Jerod Denton, Xiaohui Yan, and Kevin Strange

Departments of Anesthesiology, Molecular Physiology and Biophysics, and Pharmacology, Vanderbilt University Medical Center, Nashville, Tennessee

Submitted 30 May 2006; accepted in final form 4 August 2006

Yin X, Denton J, Yan X, Strange K. Characterization of a novel voltage-dependent outwardly rectifying anion current in *Caenorhabditis elegans* oocytes. *Am J Physiol Cell Physiol* 292: C269–C277, 2007. First published August 9, 2006; doi:10.1152/ajpcell.00298.2006.—An inwardly rectifying swelling- and meiotic cell cycle-regulated anion current carried by the ClC channel splice variant CLH-3b dominates the whole cell conductance of the *Caenorhabditis elegans* oocyte. Oocytes also express a novel outwardly rectifying anion current termed $I_{Cl,OR}$. We recently identified a worm strain carrying a null allele of the *clh-3* gene and utilized oocytes from these animals to characterize $I_{Cl,OR}$ biophysical properties. The $I_{Cl,OR}$ channel is strongly voltage dependent. Outward rectification is due to voltage-dependent current activation at depolarized voltages and rapid inactivation at voltages more hyperpolarized than approximately +20 mV. Apparent channel open probability is zero at voltages less than +20 mV. The channel has a 4:1 selectivity for Cl^- over Na^+ and an anion selectivity sequence of $SCN^- > I^- > Br^- > Cl^- > F^-$. $I_{Cl,OR}$ is relatively insensitive to most conventional anion channel inhibitors including DIDS, 4,4′-dinitrostilbene-2,2′-disulfonic acid, 9-anthracenecarboxylic acid, and 5-nitro-2-(3-phenylpropylamino)benzoic acid. However, the current is rapidly inhibited by niflumic acid, metal cations including Gd^{3+}, Cd^{2+}, and Zn^{2+}, and bath acidification. The combined biophysical properties of $I_{Cl,OR}$ are distinct from those of other anion currents that have been described. During oocyte meiotic maturation, $I_{Cl,OR}$ activity is rapidly downregulated, suggesting that the channel may play a role in oocyte Cl^- homeostasis, development, cell cycle control, and/or ovulation.

chloride channel; ovulation; cell cycle; meiotic maturation

ANION CHANNELS PLAY A VARIETY of essential physiological roles including regulation of cell excitability, transepithelial fluid transport, cell volume control, and acidification of intracellular organelles. Electrophysiological methods have identified innumerable whole cell and single-channel anion currents with diverse biophysical and regulatory properties. These currents define anion channels with conductances of a few to several hundred picosiemens that are regulated by intracellular Ca^{2+}, changes in cell volume, extracellular pH, membrane voltage, second messengers, and neurotransmitters (see, e.g., Refs. 7, 13–15, 17, 24).

Well-established families of anion channel-encoding genes include ligand-gated anion channels (4, 5, 13), ClC channels (14), and CFTR (8). At least some members of the bestrophin gene family encode anion channels (11, 22), and human homologs of the *Drosophila* gene *tweety* give rise to anion currents when expressed heterologously (23). Aquaporin 6 may also function as an anion channel in intracellular compartments (12, 25).

The limited number of anion channel-encoding genes that have been identified cannot account for the diversity of anion currents observed by electrophysiological methods. Clearly, additional anion channel-encoding genes must exit. A case in point is the channel(s) that gives rise to the outwardly rectifying swelling-activated anion current $I_{Cl,swell}$. Despite extensive study, the molecular identity of the $I_{Cl,swell}$ channel remains unknown and a source of considerable contention (9, 18, 20).

We recently began utilizing the nematode *Caenorhabditis elegans* for studies of anion channel physiology, molecular biology, and biophysics. *C. elegans* provides a number of experimental advantages for such studies (1, 21). These advantages include a short life cycle, genetic tractability, and a fully sequenced and well-annotated genome. It is also relatively easy and economical to manipulate and hence characterize gene function in *C. elegans*.

The worm oocyte is a large and relatively accessible cell type that is particularly well suited for patch-clamp electrophysiology. In wild-type oocytes, the whole cell conductance is dominated by the activity of an inwardly rectifying anion channel, CLH-3b, encoded by the ClC gene *clh-3* (6, 19). Oocytes isolated from worms harboring the *clh-3* deletion allele *ok763* lack CLH-3b currents (6), allowing us to utilize this cell type for physiological and molecular characterization of additional anion channel activity. We demonstrate here that *C. elegans* oocytes also express a novel outwardly rectifying anion current termed $I_{Cl,OR}$. $I_{Cl,OR}$ is strongly voltage dependent and is activated by depolarized voltages. Apparent open probability (P_o) of the $I_{Cl,OR}$ channel is zero at voltages more negative than approximately +20 mV. During oocyte meiotic maturation, $I_{Cl,OR}$ activity is rapidly downregulated, suggesting that the channel may play a role in oocyte ion homeostasis, development, and/or ovulation.

MATERIALS AND METHODS

C. elegans strains. The worm strain RB900, which carries the *clh-3* deletion allele *ok763*, was used throughout this study. Worms were cultured at 16°C or 20°C with standard methods (2).

Whole cell patch-clamp recording. C. elegans oocytes were isolated as described previously (19). Unless otherwise noted, experiments were performed on mix-staged, nonmaturing oocytes with cell membrane capacitances between 19 and 34 pF. Patch electrodes were pulled from 1.5-mm outer diameter silanized borosilicate microhematocrit tubes to a tip resistance of 2–4 MΩ. Whole cell currents were measured with an Axopatch 200B (Axon Instruments, Foster City,

Address for reprint requests and other correspondence: K. Strange, Vanderbilt Univ. Medical Center, T-4202 Medical Center North, Nashville, TN 37232-2520 (e-mail: kevin.strange@vanderbilt.edu).

The costs of publication of this article were defrayed in part by the payment of page charges. The article must therefore be hereby marked "*advertisement*" in accordance with 18 U.S.C. Section 1734 solely to indicate this fact.

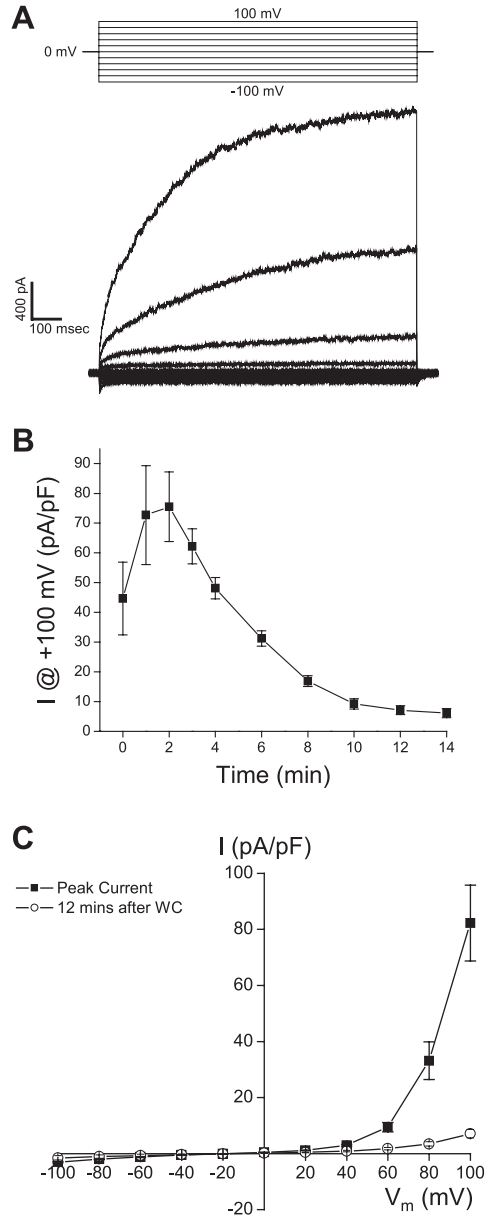

Fig. 1. Outwardly rectifying whole cell currents in oocytes isolated from *clh-3(ok763)* worms. *A*: representative whole cell current traces in a *clh-3(ok763)* oocyte. Currents were evoked by stepping membrane voltage for 1 s between −100 and +100 mV in 20-mV increments from a holding potential of 0 mV. Each test pulse was followed by a 1-s interval at 0 mV. *B*: time course of current run-up and rundown after whole cell access was obtained (*time 0*). *C*: current-voltage (*I-V*) relationships of peak whole cell current and current measured 12 min after whole cell access (WC) was achieved. Values in *B* and *C* are means ± SE (n = 5–7). V_m, membrane potential.

CA) patch-clamp amplifier. Electrical connections to the patch-clamp amplifier were made with Ag/AgCl wires and 3 M KCl/agar bridges. Data acquisition and analysis were performed with pClampfit 9.2 software (Axon Instruments). The standard bath and pipette solutions contained (mM) 140 *N*-methyl-D-glucamine (NMDG)-Cl, 2 Ca(gluconate)$_2$, 2 $MgSO_4$, 10 HEPES, and 40 sucrose (pH 7.3, 340 mosmol/kgH_2O) and 140 NMDG-Cl, 10 HEPES, and 20 sucrose (pH 7.3, 310 mosmol/kgH_2O), respectively. For studies of the pH sensitivity of whole cell currents, the bath solution was buffered with 10 mM 2-(*N*-morpholino)ethanesulfonic acid.

Statistical analyses. Data are presented as means ± SE. Statistical significance was determined with Student's two-tailed *t*-test for paired or unpaired means. P values of <0.05 were taken to indicate statistical significance.

RESULTS

clh-3(ok763) oocytes express an outwardly rectifying anion conductance. The *ok763* allele is an ~1,500-bp deletion in the *clh-3* gene. Oocytes isolated from wild-type worms express a meiotic cell cycle- and swelling-activated inwardly rectifying anion current carried by the ClC splice variant CLH-3b (6, 19). CLH-3b currents are not detected in oocytes isolated from *clh-3(ok763)* worms, indicating that *ok763* is a *clh-3*-null allele (6).

The absence of CLH-3b currents, which normally dominate whole cell recordings, enabled us to detect and characterize an outwardly rectifying conductance in *clh-3(ok763)* oocytes. As shown in Fig. 1*A*, whole cell currents were evoked by stepping

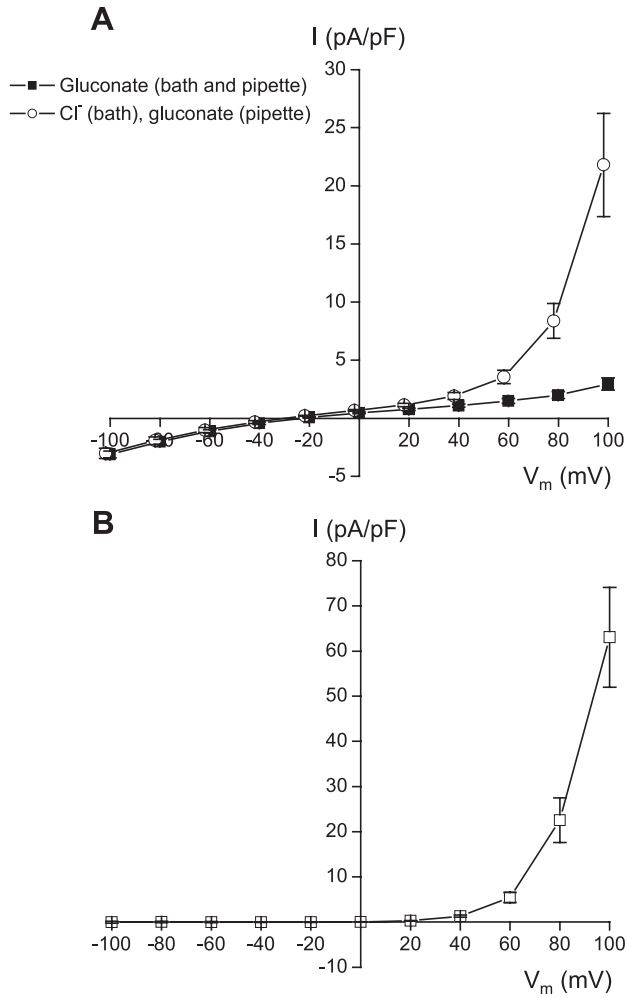

Fig. 2. Effect of Cl^- and subtraction of background current on *I-V* relationships of whole cell current amplitude and reversal potential (E_{rev}). *A*: effect of bath Cl^- on whole cell *I-V* relationships. Cells were patch clamped initially with bath and pipette solutions in which Cl^- was replaced by gluconate [■; pipette solution contained 0.1 mM *N*-methyl-D-glucamine (NMDG)-Cl to stabilize Ag-AgCl electrode]. Replacement of bath gluconate with Cl^- increases outward current ~7-fold (○). Current observed in the presence of symmetrical NMDG-gluconate solutions is defined as "background" current. Values are means ± SE (n = 5). *B*: effect of subtraction of mean background current from peak whole cell currents measured in the presence of symmetrical NMDG-Cl solutions. Values are means ± SE (n = 12).

membrane voltage for 1 s between −100 and +100 mV in 20-mV increments from a holding potential of 0 mV. At voltages greater than +60 mV, the current exhibited a time- and voltage-dependent activation (Fig. 1*A*).

The current was constitutively active on obtaining whole cell access, continued to activate for the first 1–2 min of recording, and then ran down slowly over time (Fig. 1*B*). Rundown was not prevented by addition of 100 or 420 nM Ca^{2+}, 2 mM ATP plus 2 mM Mg^{2+}, or 2 mM ATP and 0.5 mM GTP plus 2.5 mM Mg^{2+} to the pipette solution or by complete removal of Ca^{2+} (data not shown). Cell swelling or shrinkage induced by changes in bath osmolality also had no effect on current amplitude (data not shown).

Figure 1*C* shows current-voltage (*I-V*) relationships for the peak whole cell current, and the current after rundown was complete. Surprisingly, in the presence of symmetrical 140 mM NMDG-Cl bath and pipette solutions, the reversal potential (E_{rev}) of the current was strongly hyperpolarized. Mean ± SE E_{rev} values for the peak current and the current observed 12 min after obtaining whole cell access were −19 ± 2 mV (n = 7) and −23 ± 6 mV (n = 5), respectively.

Figure 2*A* shows an *I-V* relationship for cells that were patch clamped with bath and pipette solutions in which Cl^- was replaced with gluconate. Outward current was dramatically reduced under these conditions. The E_{rev} observed in the presence of symmetrical NMDG-gluconate solutions was similar to that measured in the presence of bath and pipette Cl^- (mean ± SE E_{rev} = −27 ± 1 mV; n = 21). Replacement of bath gluconate with Cl^- 3–7 min after obtaining whole cell access increased outward current approximately sevenfold at +100 mV. Bath Cl^- addition also shifted E_{rev} significantly ($P < 0.04$) from a mean ± SE value of −24 ± 3 mV to −36 ± 4 mV (n = 5). The increased current amplitude and hyperpolarizing shift in E_{rev} indicate that the outward current is carried by Cl^-.

The hyperpolarized E_{rev} of the small current observed in the presence of symmetrical NMDG-gluconate solutions can be explained by either an anion moving into the cell or a cation

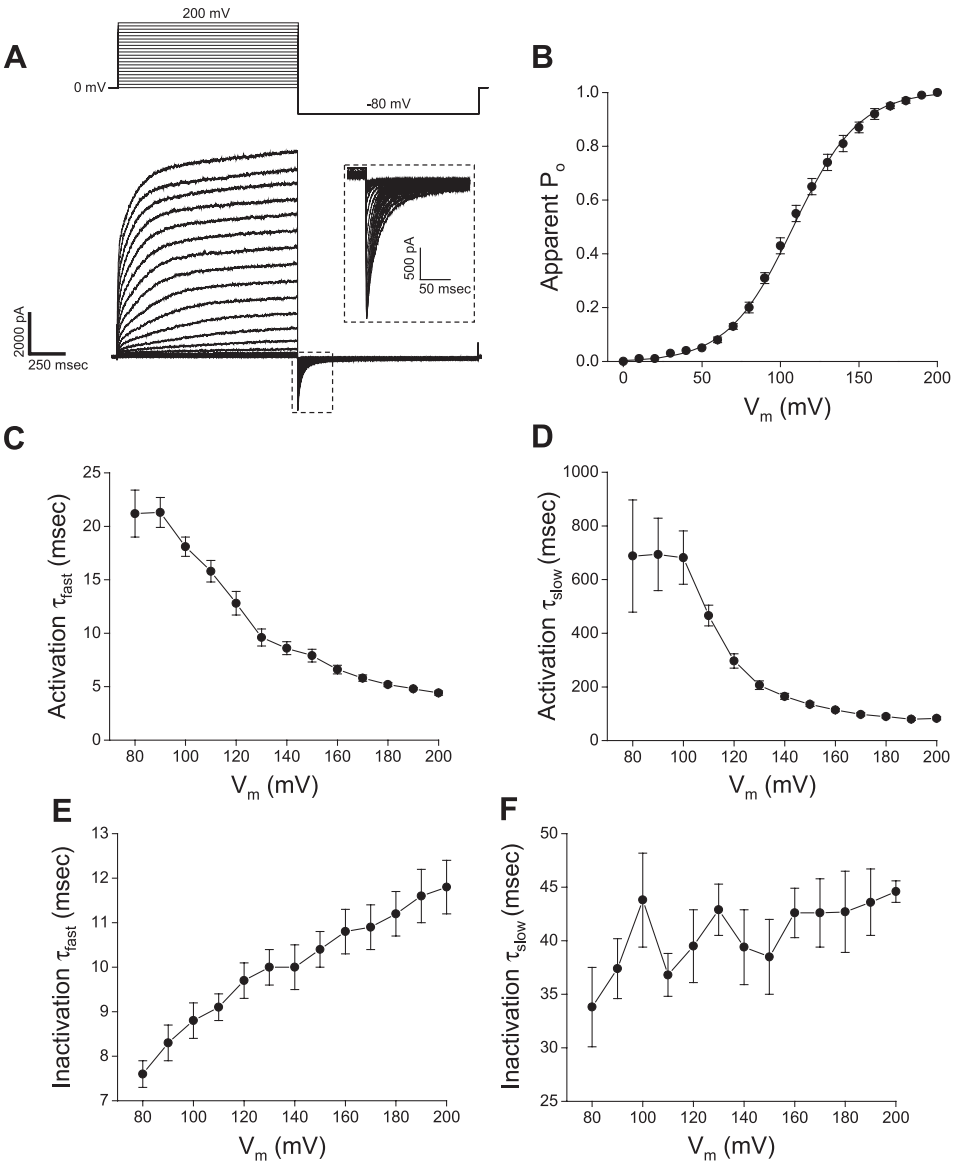

Fig. 3. Voltage-dependent properties of $I_{Cl,OR}$. *A*: representative current traces recorded during activation of $I_{Cl,OR}$ at depolarized voltages and inactivation at −80 mV. Currents were evoked by stepping membrane voltage for 1 s between 0 and +200 mV in 10-mV increments from a holding potential of 0 mV. At the end of the depolarizing step, membrane voltage was clamped to −80 mV for 1 s and then returned to 0 mV for 3 s before the next depolarizing step was initiated. Boxed region shows tail currents during inactivation at −80 mV. *B*: apparent open probability (P_o) of the $I_{Cl,OR}$ channel. P_o was estimated by plotting as a function of test voltage peak tail currents normalized to the peak tail current measured after an activating voltage step of +200 mV. Background current is defined as the peak tail current measured after a depolarizing step to 0 mV and was subtracted from peak tail currents measured at all test voltages. Values are means ± SE (n = 6). Solid line is a fit of the data with the Boltzmann function

$$P = P_{min} + \frac{P_{max} - P_{min}}{1 + e^{\frac{-zF}{RT}(V_m - V_{0.5})}}$$

where P_{max} and P_{min} are the maximum and minimum apparent P_o, respectively, z is the gating charge, F is the Faraday constant, R is the gas constant, T is the temperature, and $V_{0.5}$ is the half-maximal activation voltage. *C* and *D*: fast and slow time constants (τ) describing current activation at depolarizing voltages. Time constants were derived from double-exponential fits to whole cell currents recorded during the first 400 ms of activation. Currents elicited by voltages less than +80 mV were small, noisy, and difficult to fit with exponential functions and are therefore not included in the analysis shown here. Values are means ± SE (n = 4–7). *E* and *F*: τ_{fast} and τ_{slow} describing current inactivation at −80 mV following activation at depolarizing voltages of +80 to +200 mV. Time constants were derived from double-exponential fits to whole cell currents recorded during the first 200 ms of inactivation. Values are means ± SE (n = 6–8).

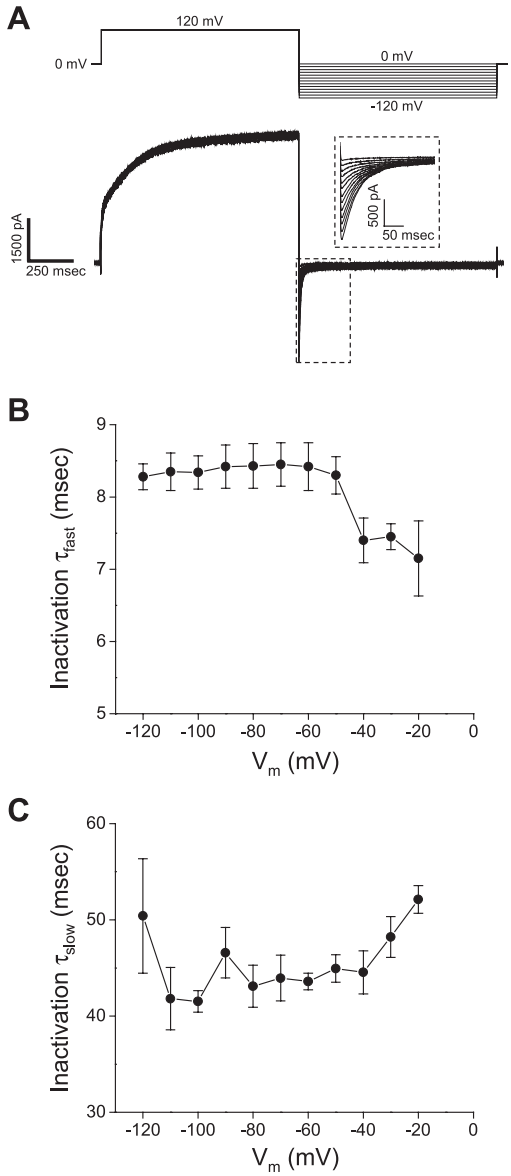

Fig. 4. Hyperpolarization-induced inactivation of $I_{Cl,OR}$. *A*: representative current traces recorded during activation of $I_{Cl,OR}$ at +120 mV and inactivation at various hyperpolarizing voltages. Currents were evoked by stepping membrane voltage for 1 s to +120 mV from a holding potential of 0 mV. To fully activate the current, the depolarizing step to +120 mV was repeated 10–20 times. After full current activation was achieved, membrane voltage was clamped for 1 s to test voltages of −120 to 0 mV. Each test voltage was followed by a 1-s step to +120 mV to reactivate the current. Boxed region shows tail currents elicited during hyperpolarizing voltage steps. *B* and *C*: τ_{fast} and τ_{slow} describing current inactivation at various hyperpolarizing voltages. Time constants were derived from double-exponential fits to whole cell currents recorded during the first 200 ms of inactivation. Values are means ± SE ($n = 6$).

moving out. The only anion other than gluconate (and OH^-) in the bath is SO_4^{2-} from 2 mM $MgSO_4$. Replacement of SO_4^{2-} with gluconate failed to depolarize E_{rev} (data not shown), indicating that inward SO_4^{2-} movement cannot account for the hyperpolarized E_{rev}.

No exogenous outwardly directed cation gradient is present in the NMDG-gluconate bath and pipette solutions. However, it is conceivable that metabolic generation of protons or organic cations produces an outwardly directed cation gradient. Reduction of extracellular pH from 7.3 to 6.3 had no significant ($P > 0.6$) effect on E_{rev} (mean ± SE E_{rev} at pH 7.3 and 6.3 = −41 ± 4 and −38 ± 5 mV, respectively; $n = 4$), suggesting that the current and hyperpolarized E_{rev} are due to the efflux from the cell of an unidentified metabolically generated organic cation. We refer to this unidentified current as a "background" current.

Figure 2*B* shows the mean *I-V* relationship of whole cell currents observed in the presence of symmetrical NMDG-Cl

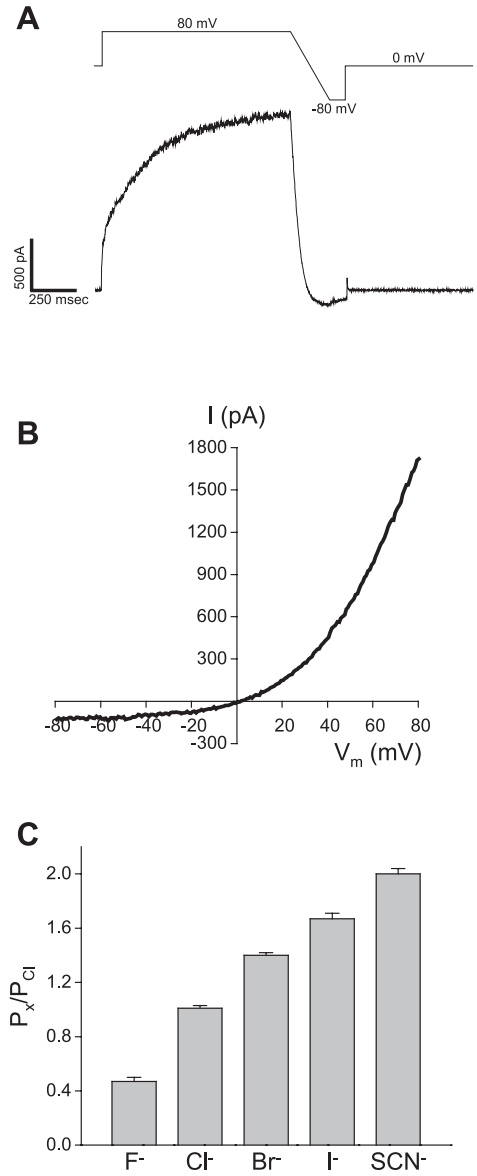

Fig. 5. Ion selectivity of the $I_{Cl,OR}$ channel. *A*: representative current traces recorded during rapid ramp protocol. $I_{Cl,OR}$ was activated by repetitive 1-s depolarizing steps to +80 mV from a holding potential of 0 mV. After stable current activation was achieved, membrane potential was ramped rapidly from +80 mV to −80 mV at 0.8 V/s. *B*: representative *I-V* relationship of $I_{Cl,OR}$ during +80 mV to −80 mV ramp. E_{rev} is close to 0 mV as expected for cells bathed and dialyzed with symmetrical 140 mM NMDG-Cl solutions. *C*: relative anion permeabilities (P_X/P_{Cl}) of the $I_{Cl,OR}$ channel. P_X/P_{Cl} values were determined with the Goldman-Hodgkin-Katz equation and the measured E_{rev} after complete replacement of bath Cl^- with the test anion. E_{rev} were corrected for liquid junction potentials calculated with pCLAMP 8. Values are means ± SE ($n = 5$ or 6).

solutions after subtraction of the mean peak background current. The background-subtracted current reversed at 1.4 ± 3.4 mV ($n = 12$), which was not significantly ($P > 0.7$) different from 0 mV. We conclude that *clh-3(ok763)* oocytes express a strongly outwardly rectifying Cl^- conductance, and we term the current carried by the channel $I_{Cl,OR}$. The $I_{Cl,OR}$ channel exhibits virtually no inward conductance when whole cell currents are evoked with the voltage step protocol shown in Fig. 1*A*. The nonzero E_{rev} observed with symmetrical NMDG-Cl solutions reflects the presence of a small inward background current that reverses at hyperpolarized voltages.

Voltage-dependent properties of $I_{Cl,OR}$. Figure 3*A* shows a family of $I_{Cl,OR}$ traces activated by 1-s depolarizing voltage steps of 0–200 mV. After each voltage step, the current was inactivated by clamping membrane voltage to −80 mV. Figure 3*A*, *inset*, shows a family of tail currents recorded during the inactivating voltage step.

The apparent P_o of the $I_{Cl,OR}$ channel at various test voltages was estimated by normalizing peak tail currents to the peak tail current measured after an activating voltage step of +200 mV. As shown in Fig. 3*B*, apparent P_o is effectively zero at voltages more negative than approximately +20 mV. The half-activation voltage and gating charge for the channel, estimated by fitting a Boltzmann function to the relative tail current data shown in Fig. 3*B*, were 107 ± 0.5 mV and −1.2 ± 0.03, respectively.

Depolarization-induced activation of $I_{Cl,OR}$ at voltages ≥80 mV was well described by the sum of two exponentials that defined fast and slow time constants (τ_{fast} and τ_{slow}). Both τ_{fast} and τ_{slow} were strongly voltage dependent and decreased with increasing depolarization (Fig. 3, *C* and *D*).

Inactivation of $I_{Cl,OR}$ at −80 mV was also described by fast and slow time constants: τ_{fast} for inactivation increased approximately twofold over the voltage range of +80 to +200 mV (Fig. 3*E*), whereas τ_{slow} was largely insensitive to activating voltage (Fig. 3*F*).

To further characterize hyperpolarization-induced inactivation, $I_{Cl,OR}$ was activated by 1-s voltage steps to +120 mV and then inactivated at test voltages of −120 mV to −20 mV (Fig. 4*A*). As shown in Fig. 4, *B* and *C*, τ_{fast} and τ_{slow} were largely insensitive to the hyperpolarizing voltages tested.

Ion selectivity of the $I_{Cl,OR}$ channel. Relative ion permeability (i.e., P_X/P_{Cl}) of the $I_{Cl,OR}$ channel was calculated with the Goldman-Hodgkin-Katz (GHK) equation and measured changes in E_{rev} induced by bath ion substitutions. Because the $I_{Cl,OR}$ channel inactivates rapidly at hyperpolarized voltages (Figs. 3 and 4), E_{rev} values could not be measured readily with step voltage-clamp protocols. Instead, $I_{Cl,OR}$ was activated by repetitive 1-s steps to +80 mV from a holding potential of 0 mV. After stable current activation was achieved, membrane potential was ramped rapidly from +80 mV to −80 mV at 0.8 V/s (Fig. 5*A*). As shown in Fig. 5*B*, significant inward current was detected with this ramp protocol. The mean ± SE E_{rev} of $I_{Cl,OR}$ measured with this ramp protocol in the presence of symmetrical 140 mM NMDG-Cl bath and pipette solutions was 0.9 ± 0.7 mV ($n = 5$). This E_{rev} was not significantly ($P > 0.3$) different from the predicted value of 0 mV.

In the presence of symmetrical 140 mM NaCl solutions, mean ± SE E_{rev} was 0.6 ± 0.9 mV ($n = 9$), which was not significantly ($P > 0.5$) different from the predicted value of 0 mV. Reduction of extracellular NaCl to 70 mM by isosmotic replacement with sucrose depolarized E_{rev} by 10.6 ± 0.4 mV ($n = 9$). The shift in E_{rev} demonstrates that the $I_{Cl,OR}$ channel is permeable to Na^+ but is predominantly anion selective. Mean ± SE relative Na^+ permeability (P_{Na}/P_{Cl}) calculated from the GHK equation was 0.25 ± 0.02 ($n = 9$).

Relative anion permeability was assessed by complete replacement of bath Cl^- with Na^+ salts of the test anion. Replacement of bath Cl^- with F^-, Br^-, I^-, or SCN^- shifted E_{rev} by 19.5 ± 0.03, −8.7 ± 0.02, −13.2 ± 0.04, and −17.8 ± 0.04 mV ($n = 5$ or 6), respectively. Calculated anion permeability ratios are shown in Fig. 5*C*. The anion selectivity sequence of the $I_{Cl,OR}$ channel is $SCN^- > I^- > Br^- > Cl^- > F^-$.

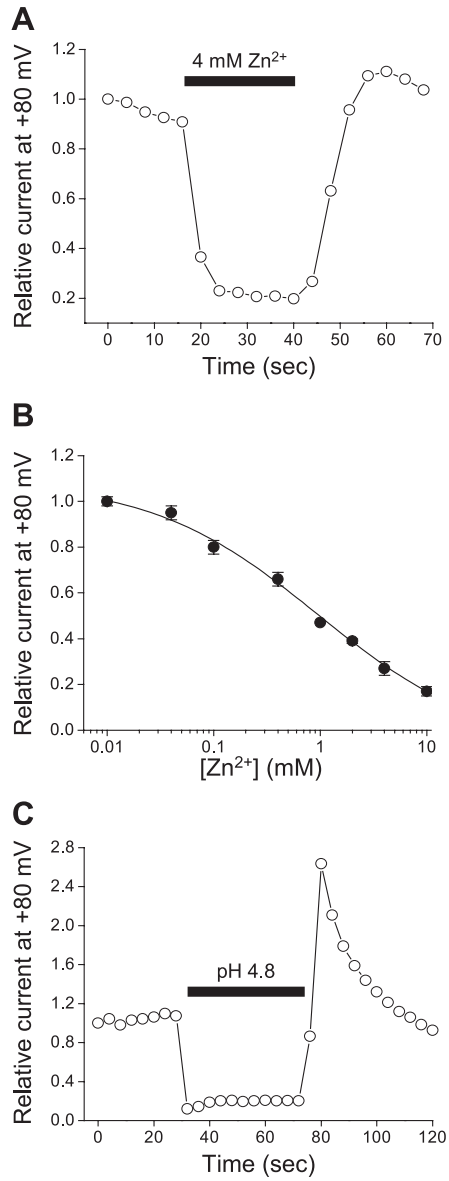

Fig. 6. Pharmacology and pH sensitivity of $I_{Cl,OR}$. *A*: effect of 4 mM Zn^{2+} on $I_{Cl,OR}$. Current was activated by repetitive 1-s depolarizing steps to +80 mV from a holding potential of 0 mV. After stable current activation was achieved, Zn^{2+} was added to the bath solution. Representative data from a single cell are shown. *B*: Hill plot of Zn^{2+} inhibition. Mean K_d and Hill coefficient for Zn^{2+} inhibition were 1.0 ± 0.3 mM and 0.6 ± 0.1, respectively. Values are means ± SE ($n = 5$ or 6). [Zn^{2+}], Zn^{2+} concentration. *C*: effect of bath acidification to pH 4.8 on $I_{Cl,OR}$ activity. Data shown are for a single cell.

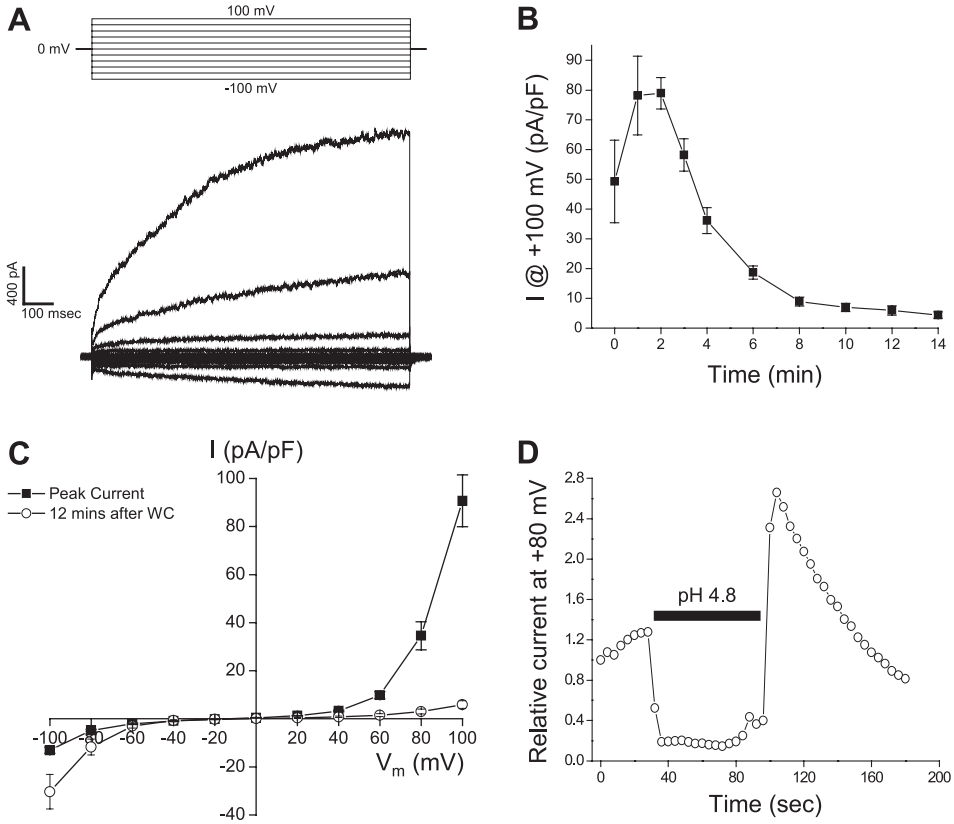

Fig. 7. Whole cell Cl^- currents in oocytes isolated from wild-type worms. *A*: representative whole cell current traces in a wild-type oocyte. Currents were evoked by stepping membrane voltage for 1 s between −100 and +100 mV in 20-mV increments from a holding potential of 0 mV. Each test pulse was followed by a 1-s interval at 0 mV. Inward current is due to the activity of CLH-3b (6, 19). *B*: time course of outwardly rectifying current run-up and rundown after whole cell access was obtained (*time 0*). Values are means ± SE (n = 6 or 7). *C*: *I-V* relationships of peak whole cell current and current measured 12 min after whole cell access was achieved. Values are means ± SE (n = 7). *D*: effect of bath acidification to pH 4.8 on outwardly rectifying current. Data shown are for a single cell.

Pharmacology and pH sensitivity of $I_{Cl,OR}$. $I_{Cl,OR}$ was not inhibited by bath addition of 0.5 mM DIDS, 0.5 mM 4,4′-dinitrostilbene-2,2′-disulfonic acid (DNDS), 0.5 mM 9-anthracenecarboxylic acid (9-AC), or 0.1 mM 5-nitro-2-(3-phenylpropylamino)benzoic acid (NPPB) (data not shown). However, 0.5 mM niflumic acid inhibited $I_{Cl,OR}$ (at +80 mV) by 50 ± 3% (n = 6). Exposure to 0.1 mM Gd^{3+}, 10 mM Cd^{2+}, or 10 mM Zn^{2+} reversibly inhibited $I_{Cl,OR}$ (at +80 mV) by 30 ± 1%

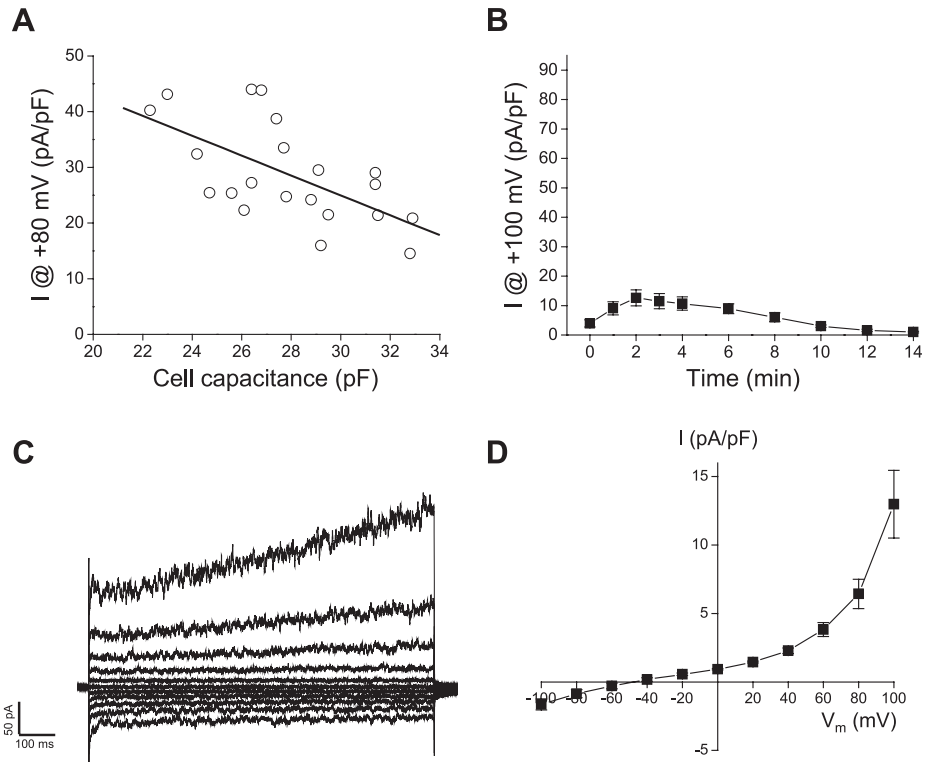

Fig. 8. Effect of oocyte development and maturation on whole cell Cl^- current. *A*: relationship between $I_{Cl,OR}$ current density and cell size, measured as whole cell capacitance, in nonmaturing oocytes. Smaller, younger oocytes have higher current density than larger, more mature oocytes. Line was determined by least-squares linear regression. Correlation coefficient (R) is −0.61. Slope is significantly ($P < 0.003$) different from zero. Currents were evoked by stepping membrane voltage for 500 ms to +80 mV every 4 s from a holding potential of 0 mV. *B*: time course of current run-up and rundown after whole cell access was obtained (*time 0*) in oocytes undergoing meiotic maturation. Currents were evoked by stepping membrane voltage for 1 s between −100 and +100 mV in 20-mV increments from a holding potential of 0 mV. Each test pulse was followed by a 1-s interval at 0 mV. For comparison, y-axis scale is the same as that shown in Fig. 1*B*. *C*: representative whole cell current traces in an oocyte undergoing meiotic maturation. Currents were evoked by stepping membrane voltage for 1 s between −100 and +100 mV in 20-mV increments from a holding potential of 0 mV. Each test pulse was followed by a 1-s interval at 0 mV. *D*: *I-V* relationships of peak whole cell current in oocytes undergoing meiotic maturation. Background current amplitude was not measured in maturing oocytes and therefore not subtracted from whole cell current traces. Values in *B* and *D* are means ± SE (n = 3–6).

($n = 6$), 78 ± 2% ($n = 6$) and 83 ± 2% ($n = 5$), respectively. Figure 6, *A* and *B*, show the effect of 4 mM Zn^{2+} on $I_{Cl,OR}$ activity and a Hill plot of Zn^{2+} inhibition. The mean ± SE K_d and Hill coefficient for Zn^{2+} inhibition were 1.0 ± 0.3 mM and 0.6 ± 0.1 ($n = 5$ or 6), respectively. Acidification of the bath to pH 4.8 rapidly and stably inhibited $I_{Cl,OR}$ by 87 ± 1% ($n = 5$; Fig. 6*C*). Current levels rapidly increased and transiently overshot initial starting levels when bath pH was increased back to pH 7.3 (Fig. 6*C*).

$I_{Cl,OR}$ is also expressed in wild-type oocytes. To determine whether $I_{Cl,OR}$ is present and might play a functional role under normal physiological conditions, we characterized outward anion currents in nonmaturing wild-type oocytes. Figure 7*A* shows wild-type oocyte whole cell currents evoked by membrane voltages between −100 and +100 mV. Inward currents activated slowly when membrane voltage was hyperpolarized to values more negative than −60 mV (Fig. 7*A*). As we have described in detail previously (6, 19), this inward current is due to the activity of CLH-3b.

Prominent outward currents were also detected in wild-type oocytes (Fig. 7*A*). Like $I_{Cl,OR}$, the outward current exhibited time- and voltage-dependent activation at voltages greater than +60 mV. Depolarization-induced activation of this current at +100 mV was well described by the sum of two exponentials that defined τ_{fast} and τ_{slow} of 14 ± 2 and 641 ± 104 ms (mean ± SE; $n = 6$), respectively. With the same voltage-clamp protocol (e.g., Figs. 1*A* and 7*A*), the fast and slow activation time constants of $I_{Cl,OR}$ in *clh-3(ok763)* oocytes were 14 ± 1 and 509 ± 94 ms (mean ± SE; $n = 6$), respectively, and were not significantly ($P > 0.5$) different from those in wild-type oocytes.

The outward current in wild-type oocytes showed a pattern of run-up and rundown that was virtually identical to that of $I_{Cl,OR}$ (Fig. 7, *B* and *C*; compare to Fig. 1, *B* and *C*) and was inhibited 44 ± 8% ($n = 3$) by addition of 1 mM Zn^{2+} to the bath. The extent of Zn^{2+} inhibition was not significantly ($P > 0.5$) different from that of $I_{Cl,OR}$ in *clh-3(ok763)* oocytes (see Fig. 6*B*). The outward current was also inhibited by bath acidification (Fig. 7*D*). Mean ± SE percent inhibition was 86 ± 1% ($n = 4$), which was not significantly ($P > 0.5$) different from that observed for $I_{Cl,OR}$. When bath pH was increased back to pH 7.3, current levels rapidly increased and transiently overshot their initial starting levels (Fig. 7*D*). This rapid recovery and overshoot were also observed in oocytes isolated from *clh-3(ok763)* worms (see Fig. 6*C*). On the basis of the results shown in Fig. 7 and discussed above, we conclude that $I_{Cl,OR}$ is expressed and functional in wild-type oocytes.

Developmental regulation of $I_{Cl,OR}$ activity. Adult *C. elegans* hermaphrodites possess two U-shaped gonad arms connected via spermatheca to a common uterus. Oocytes form in the proximal gonad and accumulate in a single-file row of graded developmental stages. Developing oocytes remain in diakinesis of prophase I until they reach the most proximal position in the gonad arm, where they reenter the meiotic cell cycle, a process termed meiotic maturation. Maturing oocytes are ovulated into the spermatheca for fertilization. During development and progression through the gonad, oocyte size increases ~200-fold before initiation of meiotic maturation and ovulation (10, 16).

As shown in Fig. 8*A*, oocyte size, which reflects oocyte developmental stage, was inversely correlated with $I_{Cl,OR}$ current density. Smaller, younger oocytes exhibited higher current densities compared with larger, more fully developed oocytes. In fully grown oocytes undergoing meiotic maturation, peak current levels were six- to sevenfold lower ($P < 0.001$) than those observed in oocytes at earlier stages of development (Fig. 8*B*).

Whole cell current in maturing oocytes underwent a run-up and rundown that was similar to $I_{Cl,OR}$ observed in nonmaturing cells (compare Figs. 1*B* and 7*B*). However, the voltage-dependent properties of the current in maturing oocytes were considerably different. Instantaneous currents were detected at depolarized voltages, and these currents exhibited a slow linear time-dependent activation (compare Figs. 1*A* and 7*C*). In addition, the current was less rectified than that observed in nonmaturing oocytes (compare Figs. 1*C* and 7*D*).

We examined the ion selectivity and pharmacological properties of the current in maturing oocytes to assess whether they

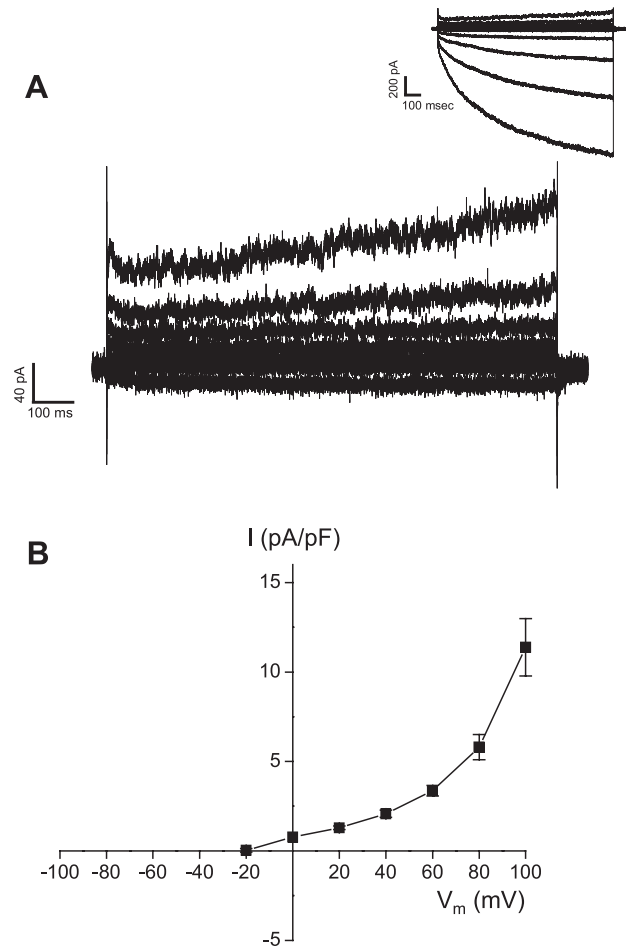

Fig. 9. Whole cell Cl^- currents in wild-type oocytes undergoing meiotic maturation. *A*: representative whole cell current traces. Currents were evoked by stepping membrane voltage for 1 s between −100 and +100 mV in 20-mV increments from a holding potential of 0 mV. Each test pulse was followed by a 1-s interval at 0 mV. To facilitate comparison to Fig. 8*C*, currents are shown only between −20 and +100 mV. *Inset*, currents from −100 to +100 mV. Inward current is due to the activity of CLH-3b, which is activated during meiotic maturation (6, 19). *B*: *I-V* relationships of peak outward whole cell currents at −20 to +100 mV. Values are means ± SE ($n = 5$).

were carried by the $I_{Cl,OR}$ channel. Reduction of extracellular NaCl to 70 mM depolarized E_{rev} by 12.4 ± 0.6 mV (n = 6). The mean ± SE calculated P_{Na}/P_{Cl} of the channel was 0.17 ± 0.02. Replacement of extracellular Cl^- with F^-, Br^-, I^-, or SCN^- shifted E_{rev} by 26.3 ± 1.7, −6.9 ± 0.5, −11.9 ± 0.2, and −19.1 ± 0.7 mV, respectively (n = 5 or 6). Mean ± SE anion P_X/P_{Cl} for F^-, Br^-, I^-, and SCN^- were 0.36 ± 0.03, 1.31 ± 0.03, 1.59 ± 0.01, and 2.11 ± 0.06 (n = 5 or 6), respectively, which yields an anion selectivity sequence of $SCN^- > I^- > Br^- > Cl^- > F^-$. Addition of 10 mM Zn^{2+} or 0.5 mM niflumic acid to the bath inhibited the current by 68 ± 4% (n = 4) and 75 ± 7% (n = 3), respectively. As with the current in nonmaturing oocytes, bath addition of DIDS, 9-AC, or NPPB had no inhibitory effect (data not shown). The cation selectivity, anion selectivity, and pharmacological properties of the outward Cl^- currents in maturing oocytes are similar to those in nonmaturing oocytes, indicating that they are carried by the $I_{Cl,OR}$ channel.

We also examined whole cell currents in wild-type oocytes undergoing meiotic maturation. $I_{Cl,OR}$ in maturing wild-type oocytes showed the same pattern of change, including altered voltage-dependent activation (Fig. 9*A*) and a six- to sevenfold reduction in amplitude (Fig. 9*B*). The current also underwent run-up and rundown similar to that observed in *clh-3(ok763)* oocytes (data not shown).

DISCUSSION

Our patch-clamp studies on oocytes isolated from wild-type and a *clh-3*-null mutant worm strain have identified a novel outwardly rectifying anion current, $I_{Cl,OR}$. The strong outward rectification of $I_{Cl,OR}$ is due to voltage-dependent current activation at depolarized voltages and rapid inactivation at voltages more hyperpolarized than approximately +20 mV (Figs. 3 and 4). The $I_{Cl,OR}$ channel has a 4:1 selectivity for anions over cations and an anion selectivity sequence of $SCN^- > I^- > Br^- > Cl^- > F^-$ (Fig. 5). $I_{Cl,OR}$ is relatively insensitive to most conventional anion channel inhibitors including DIDS, DNDS, 9-AC, and NPPB. However, the current is rapidly inhibited by niflumic acid and metal cations including Gd^{3+}, Cd^{2+}, and Zn^{2+} (see e.g., Fig. 6, *A* and *B*). Bath acidification also inhibits the current (Fig. 6*C*).

The combined biophysical properties of $I_{Cl,OR}$ are distinct from those of other anion currents that have been described. However, two recently characterized anion currents, $I_{Cl,mec}$ and $I_{Cl,acid}$, bear some similarity to $I_{Cl,OR}$. $I_{Cl,acid}$ is a strongly outwardly rectifying anion current identified in HEK293 cells (15). The $I_{Cl,acid}$ and $I_{Cl,OR}$ channels have similar voltage-dependent properties and anion selectivities but differ sharply in their pharmacology. In addition, $I_{Cl,acid}$ is activated by protons, whereas protons inhibit $I_{Cl,OR}$.

$I_{Cl,mec}$ is a strongly outwardly rectifying anion current present in developing *C. elegans* embryo cells that is activated by membrane stretch (3). The $I_{Cl,mec}$ and $I_{Cl,OR}$ channels have similar voltage-dependent properties and nearly identical relative cation and anion permeabilities. However, $I_{Cl,mec}$ is inhibited by both DIDS and NPPB, and membrane stretch induced by oocyte swelling or shrinkage had no consistent effect on $I_{Cl,OR}$ activity.

The molecular identity of the $I_{Cl,OR}$ channel is uncertain at present. None of the identified anion channel genes encodes channels with functional properties that recapitulate those of $I_{Cl,OR}$. Some ClC genes give rise to strongly outwardly rectifying currents (14), but the $I_{Cl,OR}$ channel is almost certainly not a ClC. Six ClC genes termed *clh-1* through *-6* are present in the worm genome. Oocytes isolated from worms harboring deletion alleles for *clh-1*, *clh-2*, *clh-4*, or *clh-6* expressed normal $I_{Cl,OR}$ activity and RT-PCR-confirmed knockdown of *clh-5* expression by RNA interference (RNAi) had no effect on $I_{Cl,OR}$ amplitude (data not shown). In addition, RNAi directed at *clh-3(ok763)* mRNA did not alter current properties, indicating that the $I_{Cl,OR}$ channel is not encoded by the mutant *clh-3* gene (data not shown). Additional functional and molecular studies are required to identify the gene(s) encoding the $I_{Cl,OR}$ channel.

As shown in Figs. 8 and 9, $I_{Cl,OR}$ activity is dramatically reduced in oocytes undergoing meiotic maturation. Interestingly, CLH-3b and $I_{Cl,mec}$ also show striking changes in activity during oocyte and early embryo development. CLH-3b is activated specifically during oocyte meiotic maturation and plays a role in regulating ovulation (19, 26). Membrane expression of CLH-3b is detected throughout all stages of oocyte development (6). However, within minutes after ovulation occurs, the channel is rapidly lost from the plasma membrane and expression of the *clh-3* gene is not detected again until very late in embryonic development (unpublished observations). In contrast to CLH-3b, $I_{Cl,mec}$ appears to be activated shortly after embryogenesis begins. High levels of $I_{Cl,mec}$ activity are present in developing embryo cells as early as the 1- and 2-cell stages, but the current cannot be detected in oocytes (3).

The likely role of CLH-3b is to regulate oocyte membrane potential, which in turn may modulate Ca^{2+} signaling in the surrounding gap junction coupled sheath cells (19, 26). $I_{Cl,OR}$ may also play a role in regulating membrane potential. Such regulation could in turn serve to control oocyte development, ovulation, and/or cell cycle progression. Alternatively, $I_{Cl,OR}$ may have a general housekeeping function and participate in intracellular Cl^- homeostasis required for proper cell volume and acid-base control. Identification of the gene(s) that encodes the $I_{Cl,OR}$ channel will be facilitated by the molecular and genetic tractability of *C. elegans* and is essential in order to fully define channel function and regulation.

GRANTS

This work was supported by National Institutes of Health (NIH) Grant DK-51610 to K. Strange. Worm strains were obtained from the *Caenorhabditis* Genetics Center, which is supported by the NIH National Center for Research Resources.

REFERENCES

1. **Barr MM.** Super models. *Physiol Genomics* 13: 15–24, 2003.
2. **Brenner S.** The genetics of *Caenorhabditis elegans*. *Genetics* 77: 71–94, 1974.
3. **Christensen M, Strange K.** Developmental regulation of a novel outwardly rectifying mechanosensitive anion channel in *Caenorhabditis elegans*. *J Biol Chem* 276: 45024–45030, 2001.
4. **Dent JA, Davis MW, Avery L.** *avr-15* encodes a chloride channel subunit that mediates inhibitory glutamatergic neurotransmission and ivermectin sensitivity in *Caenorhabditis elegans*. *EMBO J* 16: 5867–5879, 1997.
5. **Dent JA, Smith MM, Vassilatis DK, Avery L.** The genetics of ivermectin resistance in *Caenorhabditis elegans*. *Proc Natl Acad Sci USA* 97: 2674–2679, 2000.
6. **Denton J, Nehrke K, Rutledge E, Morrison R, Strange K.** Alternative splicing of N- and C-termini of a *C. elegans* ClC channel alters gating and sensitivity to external Cl^- and H^+. *J Physiol* 555: 97–114, 2004.

7. **Frings S, Reuter D, Kleene SJ.** Neuronal Ca^{2+}-activated Cl^- channels—homing in on an elusive channel species. *Prog Neurobiol* 60: 247–289, 2000.
8. **Gadsby DC, Vergani P, Csanady L.** The ABC protein turned chloride channel whose failure causes cystic fibrosis. *Nature* 440: 477–483, 2006.
9. **Greenwood IA.** CLC-3 knockout hints at swelling-activated chloride channel complexity. *J Physiol* 557: 343, 2004.
10. **Hall DH, Winfrey VP, Blaeuer G, Hoffman LH, Furuta T, Rose KL, Hobert O, Greenstein D.** Ultrastructural features of the adult hermaphrodite gonad of *Caenorhabditis elegans*: relations between the germ line and soma. *Dev Biol* 212: 101–123, 1999.
11. **Hartzell C, Qu Z, Putzier I, Artinian L, Chien LT, Cui Y.** Looking chloride channels straight in the eye: bestrophins, lipofuscinosis, and retinal degeneration. *Physiology* 20: 292–302, 2005.
12. **Hazama A, Kozono D, Guggino WB, Agre P, Yasui M.** Ion permeation of AQP6 water channel protein. Single channel recordings after Hg^{2+} activation. *J Biol Chem* 277: 29224–29230, 2002.
13. **Jackson MB.** Ligand-gated channel: postsynaptic receptors and drug targets. *Adv Neurol* 79: 511–524, 1999.
14. **Jentsch TJ, Neagoe I, Scheel O.** CLC chloride channels and transporters. *Curr Opin Neurobiol* 15: 319–325, 2005.
15. **Lambert S, Oberwinkler J.** Characterization of a proton-activated, outwardly rectifying anion channel. *J Physiol* 567: 191–213, 2005.
16. **McCarter J, Bartlett B, Dang T, Schedl T.** On the control of oocyte meiotic maturation and ovulation in *Caenorhabditis elegans*. *Dev Biol* 205: 111–128, 1999.
17. **Morris AP.** The regulation of epithelial cell cAMP- and calcium-dependent chloride channels. *Adv Pharmacol* 46: 209–251, 1999.
18. **Okada Y.** Volume expansion-sensing outward-rectifier Cl^- channel: fresh start to the molecular identity and volume sensor. *Am J Physiol Cell Physiol* 273: C755–C789, 1997.
19. **Rutledge E, Bianchi L, Christensen M, Boehmer C, Morrison R, Broslat A, Beld AM, George A, Greenstein D, Strange K.** CLH-3, a ClC-2 anion channel ortholog activated during meiotic maturation in *C. elegans* oocytes. *Curr Biol* 11: 161–170, 2001.
20. **Strange K.** Molecular identity of the outwardly rectifying, swelling-activated anion channel: time to re-evaluate pICln. *J Gen Physiol* 111: 617–622, 1998.
21. **Strange K.** From genes to integrative physiology: ion channel and transporter biology in *Caenorhabditis elegans*. *Physiol Rev* 83: 377–415, 2003.
22. **Sun H, Tsunenari T, Yau KW, Nathans J.** The vitelliform macular dystrophy protein defines a new family of chloride channels. *Proc Natl Acad Sci USA* 99: 4008–4013, 2002.
23. **Suzuki M, Mizuno A.** A novel human Cl^- channel family related to *Drosophila flightless* locus. *J Biol Chem* 279: 22461–22468, 2004.
24. **Suzuki M, Morita T, Iwamoto T.** Diversity of Cl^- channels. *Cell Mol Life Sci* 63: 12–24, 2006.
25. **Yasui M, Hazama A, Kwon TH, Nielsen S, Guggino WB, Agre P.** Rapid gating and anion permeability of an intracellular aquaporin. *Nature* 402: 184–187, 1999.
26. **Yin X, Gower NJ, Baylis HA, Strange K.** Inositol 1,4,5-trisphosphate signaling regulates rhythmic contractile activity of smooth muscle-like sheath cells in the nematode *Caenorhabditis elegans*. *Mol Biol Cell* 15: 3938–3949, 2004.